Schmidt, W., Berthelot, R., Sleight, A., & Subramanian, M. (2013). Solid solution studies of layered honeycomb-ordered phases O3-$Na_3M_2SbO_6$ (M = Cu, Mg, Ni, Zn). Journal of Solid State Chemistry, 201, 178-185. doi:10.1016/j.jssc.2013.02.035

# Solid Solution Studies of Layered Honeycomb-Ordered Phases O3-$Na_3M_2SbO_6$ (M = Cu, Mg, Ni, Zn)

Whitney Schmidt, Romain Berthelot, A. W. Sleight, M. A. Subramanian*

*Department of Chemistry, Oregon State University, Corvallis, OR 97331, USA*

**Abstract:**

Complete solid solutions with the composition $Na_3M_{2-x}M'_xSbO_6$ where M, M' = Cu, Mg, Ni, Zn have been synthesized by conventional solid state techniques and were investigated using X-ray diffraction, magnetism and optical measurements. All compositions crystallize in a monoclinic unit cell and exhibit a layered structure with a honeycomb cationic ordering within the slabs. These compounds also exhibit Curie-Weiss behavior at high temperatures and the magnetic moment values verify the presence of $Cu^{2+}$ and/or $Ni^{2+}$. The antiferromagnetic order of $Na_3Ni_2SbO_6$ is suppressed upon substitution of $Ni^{2+}$ with $Mg^{2+}$ or $Zn^{2+}$. The spin gap observed in $Na_3Cu_2SbO_6$ is also suppressed by substitution of $Cu^{2+}$ with $Mg^{2+}$ or $Zn^{2+}$. The $Na_3Ni_{2-x}Cu_xSbO_6$ compositions follow an expected transition from an antiferromagnetic ordering to the spin gap of the copper end member. The estimated band gaps for these compounds have been estimated from diffuse reflectance measurements.

**Keywords**

Layered compound, Honeycomb ordering, Solid solution, X-ray diffraction, Spin-gap behavior

*Corresponding author: mas.subramanian@oregonstate.edu,

Department of Chemistry
Oregon State University
153 Gilbert Hall
Corvallis, OR 97331
(541)-737-8235

**1. Introduction:**

Layered ternary oxides $AMO_2$, with M a transition metal and A an alkali, include a wide number of compounds that have been extensively studied because of their remarkable chemical and physical properties. As alkali ions can be reversibly deintercalated from the layered structure, their main interest is their electrochemical behavior as positive electrode materials for lithium-ion or sodium-ion batteries.[1–7] $LiCoO_2$ is nowadays the reference oxide for positive electrode materials of lithium batteries.[6,7] The reports of other interesting physical behaviors have focused the interest of the scientific community on these layered alkali-transition metal oxides. For example, the unexpected thermoelectric behavior for $Na_xCoO_2$ with high sodium content or the superconductivity in hydrated $Na_xCoO_2 \bullet yH_2O$ phases.[8,9]

The layered structure of these alkali-transition metal oxides is one of the key points that explain all of these fascinating properties. The structure is usually described as a stacking of $MO_2$ slabs of edge-sharing $MO_6$ octahedra. Depending on the overall chemical formula $A_xMO_2$ and the synthesis conditions, different stacking sequences of the $MO_2$ slabs are available, which involve different intercalation site symmetries for A: octahedral, trigonal prismatic, tetrahedral or linear. In order to clearly identify the stacking sequences of these materials, a specific nomenclature can be used which consists of a letter that links the intercalation site symmetry (*i.e.* O for octahedral) and a numeral corresponding to the number of $MO_2$ slabs in the hexagonal unit cell.[10]

While keeping the general layered structure of the $AMO_2$ compounds, a large number of other compounds have been reported in the literature by substituting the M cation with another X cation. Specifically when only 1/3 of M is substituted by X, the general formula is expanded to $A_2M_2XO_6$ and $A_3M_2XO_6$, where M is now a 2+ cation and the A content is dependent on the oxidation state of the X cation (usually 5+ or 6+). These specific compositions sometimes lead to a M/X cationic ordering within the slab. Indeed each $XO_6$ octahedron is therefore surrounded by six $MO_6$ octahedra forming a

honeycomb network. Many compositions have already been reported in the literature: $A_3M_2XO_6$ (A = Na, Li; X = Sb, Bi, Nb, Ta, Ru) or $A_2M_2TeO_6$ (M = Co, Cu, Mg, Zn, Ni).[11–30] Greaves *et al*. first reported on the $Li_3Zn_2XO_6$ (X = Bi, Sb) compositions.[11] Since then, the antimony containing phases have expanded to include many compositions ($A_3M_2SbO_6$, A = Li, Na, Ag, Cu; M = Co, Cu, Mg, Ni, Zn).[12,13,15–19,21,22,24] In particular, $A_3Cu_2SbO_6$ (A = Cu, Na, Li) have been the more heavily studied materials due to interesting magnetic properties, such as a spin gap behavior which results from the $d^9$ $Cu^{2+}$ in the honeycomb arrangement. From a structural point, the copper containing compounds show interesting trends due to distorted $CuO_6$ octahedra from the Jahn-Teller active $Cu^{2+}$.[12,16,18,22] The $A_3Ni_2XO_6$ compositions have also been discussed regarding their magnetic and structural properties which arise from the $d^8$ $Ni^{2+}$. These $Ni^{2+}$ containing compounds usually show low temperature antiferromagnetic behavior in which the Néel temperature shifts depending on the nature of the X cation.[17,21,24,25]

In our group we recently studied the solid solutions between P2-$Na_2M_2TeO_6$ compounds where M = Co, Ni, Zn. As it was previously showed by Evstigneeva *et al.*[23], the nickel containing compound possesses a different stacking sequence of the slabs than that of the cobalt and zinc compounds. This causes a structural transition from the nickel (space group $P6_3/mcm$) to the cobalt or zinc (space group $P6_322$) compounds.[26] We also reported the new compound O3-$Li_3Ni_2BiO_6$ and studied the O3-$Li_3NiMBiO_6$ (M = Mg, Cu, Zn) intermediate compositions. When copper is substituted, the lattice parameters of the *C2/*m space group did not follow the general trend with the other compositions only based on a simple ionic radius explanation. The β angle of the monoclinic cell became larger with the *a* and *c* parameters increasing and the *b* parameter decreasing more significantly than the trend related to the ionic sizes of the metal cations.

In this present study we focused our interest on the O3-$Na_3M_2SbO_6$ compounds and studied the solid solutions for M = Cu, Mg, Ni, Zn. As it is described above, the $SbO_6$ octahedron is surrounded by six $MO_6$

edge-sharing octahedra forming the honeycomb lattice (Figure 1). The $Na^+$ ions are intercalated within the $M_2SbO_6$ slabs and occupy an octahedral $NaO_6$ site. These compounds were synthesized using solid state method and were characterized using X-ray diffraction, magnetic susceptibility and diffuse reflectance. This is the first report of solid solutions of these compositions and the first report of optical studies on these compounds.

**2. Experimental:**

Polycrystalline powder samples were prepared by solid state synthesis techniques. Sodium carbonate ($Na_2CO_3$, Spectrum Chemical 99.5%), antimony oxide ($Sb_2O_3$, J. T. Baker highly pure), copper oxide (CuO, Aldrich 99.99%), magnesium oxide (MgO, Alfa Aesar 99.95%), nickel oxide (NiO, Alfa Aesar 99.998%) and zinc oxide (ZnO, Aldrich 99.9%) were thoroughly ground together in the desired stoichiometric proportions. The sodium carbonate and the magnesium oxide were dried (120 °C and 900 °C respectively) prior to weighing to prevent moisture contamination. The pelletized samples were loaded onto an Au tray which was placed in an alumina boat. The samples were heated two times for 12 hrs at 900 °C (ramp rate of 5 °C $min^{-1}$) with intermediate grinding. After the heat treatment, the furnace was switched off and allowed to cool to room temperature before removal of the samples.

X-ray diffraction (XRD) measurements were carried out on a Rigaku Miniflex II diffractometer using Cu Kα radiation and a graphite monochromator on the diffracted beam. The powder samples were loaded on an oriented Si single crystal zero background sample holder (MTI corp.). Measurements were collected from 10 – 80° 2θ (steps of 0.02°) with a 2 s fixed time. Profile matching using the Le Bail method were performed with the FullProf Suite including the WinPLOTR tool.[31–33]

Magnetic susceptibility measurements were carried out on a Quantum Design physical property measurement system (PPMS). Measurements were collected from 5 – 300K under a 1T field and zero-field cooled conditions.

Diffuse reflectance measurements were carried out on packed powder samples using a halogen source (200 – 1150 nm) passed through bifurcated fiber optic wire and MgO (Sigma Aldrich, 99.9%) as the white reference. The data was collected on an Ocean Optics HR4000 spectrophotometer. The collected data was converted to absorbance using the Kubelka-Munk relation.[34]

**3. Results and Discussion:**

*3.1 XRD studies of O3-$Na_3M_2SbO_6$ (M = Cu, Mg, Ni, Zn) and the solid solutions:*

The powder X-ray diffraction (PXRD) patterns for the compositions $Na_3M_2SbO_6$ (M = Cu, Mg, Ni, Zn) are shown in Figure 2. All of the patterns were indexed to the monoclinic space group *C2/m* and there were no traces of impurity phases. The refined lattice parameters are listed in Table 1. When M = Mg, Ni and Zn, the lattice parameters agree well with reported values (Table 1) and they also follow an expected trend based on the radii of the $M^{2+}$ ion ($Ni^{2+}$ = 0.69 Å, $Mg^{2+}$ = 0.72 Å and $Zn^{2+}$ = 0.74 Å).[35] Therefore there is only a slightly visible shifting of the *hkl* reflections which can be seen in Figure 2. It has been reported that these honeycomb layered materials can also be indexed using the $P3_112$ or the *C2/c* space groups;[16,21] however Bréger *et al*. report that the *C2/m* space group has the lowest calculated energy for the ordered honeycomb compounds.[36] With an ionic radius of 0.73 Å, it would be assumed that the lattice parameters for $Na_3Cu_2SbO_6$ would fall between those of the magnesium and zinc compositions. The copper composition however, has larger *a* and *c* lattice parameters, a smaller *b* lattice parameter and a much larger β angle than the other compositions. The PXRD pattern in Figure 2 indicates this difference with the shifted reflections of the monoclinic cell. This deviation from a linear trend cannot be explained by using the ionic radii. This change in the lattice constant trend is attributed to the Jahn-Teller (J-T) distortion that can occur with $Cu^{2+}$ in an octahedral coordination.[16] The J-T distortion of $CuO_6$ octahedra results in an axial extension and an equatorial compression of Cu – O bonds. As is seen in Figure 1, the $MO_6$ octahedra sit on a face and share edges with the other octahedra throughout the $M_2SbO_6$ slabs. The axial extension of the $CuO_6$ octahedron results in the smaller *b*

parameter and the equatorial compression results in the larger *a* and *c* lattice parameters. This also creates the larger β angle and the highly shifted *hkl* reflections of the $Na_3Cu_2SbO_6$ composition. This Jahn-Teller structural distortion has been observed in other compounds containing copper, such as $Li_3NiCuBiO_6$ and $Li_3Cu_2SbO_6$.[12,25,28]

It is noticed that the reflections in the PXRD patterns between 17° and 30° 2θ are very weak for the $Zn^{2+}$ and $Ni^{2+}$ compounds. The crystallinity of our compounds may have been hindered by our use of slightly lower temperature than that reported by Politaev *et al*. for synthesis. This did not however affect our profile matching to the *C2/m* space group. This 2θ region is also where stacking faults affect the resolution of the *hkl* reflections and create an asymmetric broadening of the affected reflections. The phenomenon is easily noticed in the PXRD pattern of the magnesium composition (Figure 2). This broadening is described as stacking defects along the monoclinic *c* axis and is present in the $Na_3Ni_2SbO_6$[21] parent compound as well as in other related "honeycomb" layered materials, e.g. in $Li_2MnO_3$.[36,37] These stacking faults arise in layered structures because of a variety of stacking sequences available for each layer which affects the intercalation site symmetry for the interslab ions as discussed earlier. The calculated energies reported for the different stacking sequences of the $P3_112$ and the *C2/c* are only 1 meV and 2 meV per formula unit, respectively, higher than that of the *C2/m* space group.[36] Such closely related energies will result in stacking faults to arise in the layered structures. Breger *et al.* found that in the $Li_2MnO_3$ compounds, the annealing time decreased the stacking faults more so than the annealing temperature and related these fault formations to slow kinetics of growth along the *c* direction. Due to the presence of stacking faults, it is difficult for Rietveld refinement therefore; the reported lattice parameters in this work are from Le Bail profile refinement using a Pseudo-Voigt function.

As pure end members were obtained with similar experimental parameters, it is therefore reasonable to synthesize the intermediate compositions $Na_3M_{2-x}M'_xSbO_6$ (M, M' = Cu, Mg, Ni, Zn; $0 \leq x \leq 2$). As a

general case and in order to lighten the study, only the PXRD for the solid solutions $Na_3Ni_{2-x}Mg_xSbO_6$ and $Na_3Cu_{2-x}Zn_xSbO_6$ are shown in Figures 3 and 4 respectively. As expected, the *a, b* and *c* parameters only slightly shift in a linear fashion due to the radii of the cations while the β angle is constant at approximately 108° for M = Ni, Mg, Zn. Indeed the unit cell increases from 259 $Å^3$ (for $Ni^{2+}$, 0.69 Å), 263 $Å^3$ (for $Mg^{2+}$, 0.72 Å) and 267 $Å^3$ (for $Zn^{2+}$, 0.74 Å).[35]

The solid solutions containing copper were also synthesized without impurity however the lattice parameters change more dramatically along the $Na_3Cu_{2-x}M_xSbO_6$ (M = Mg, Ni, Zn) series than those for the solid solutions not containing copper. As an example, the PXRD patterns for the series $Na_3Cu_{2-x}Zn_xSbO_6$ are shown in Figure 4. In $Na_3Cu_2SbO_6$, the $Cu^{2+}$ is Jahn-Teller active which results in an elongation of the axial Cu – O bonds (affecting the *b* axis) and a contraction of the equatorial Cu – O bonds (affecting the *a* and *c* axes). The stretching of the axial bonds and contraction of the equatorial bonds in the $CuO_6$ octahedra cause the β angle to become larger than that of the other $M^{2+}$ compounds. The lattice parameter and β angle shifts are presented in Figure 5. This trend related to the J-T activity of $Cu^{2+}$ was previously noted in the similar phase $Li_3NiCuBiO_6$.[25] Dilution of the J-T active $Cu^{2+}$ reduces the distortion in the $M_2SbO_6$ slabs. Therefore, the specific *hkl* reflections that are involved in the transition from the regular $ZnO_6$ octahedra to the distortion of the J-T $CuO_6$ octahedra clearly shifts along the solid solution $Na_3Cu_{2-x}Zn_xSbO_6$.

It is interesting to note that in all the studied solid solutions, no superstructure reflections due to additional ordering between M and M' cations were evidenced. Due to similar scattering factors, it would be difficult to detect such superstructure reflections between the compounds containing Cu, Ni and Zn. The linear trend of the lattice parameters indicates that any cation ordering would be unlikely.

*3.2 Magnetic Susceptibility:*

It is interesting to study the magnetic properties as $Ni^{2+}$ ($3d^8$) and $Cu^{2+}$ ($3d^9$) have complex magnetic interactions depending on the nearest neighbors in the honeycomb ordering of these compounds.

Previous reports indicate a spin gap behavior in $Na_3Cu_2SbO_6$, which is also present in the delafossite phase $Cu_5SbO_6$ (*i.e.* $Cu_3Cu_2SbO_6$) and O3-$Na_2Cu_2TeO_6$, due to Cu – Cu dimer formation in the $Cu_2SbO_6$ honeycomb layers.[18,22,38–40] Due to the honeycomb ordering of the $Cu_2SbO_6$ slabs and the Jahn-Teller distortion of the $CuO_6$ octahedra, two copper neighbors come close enough to form $Cu_2O_{10}$ dimers. The magnetic susceptibility plot can be seen in Figure 6 and shows a broad maximum at ~90 K, indicative of a spin gap behavior.[16,18,22,40] The high temperature data follows the Curie-Weiss law and was fit with $\chi = C/(T - \theta)$ between 150 and 300 K which revealed $\mu_{eff}$ = 2.55 μB and θ = -23 K. This effective magnetic moment is in agreement with the calculated theoretical magnetic moment $\mu_{theor}$ = 2.45 $\mu_B$.

There is no report on the magnetic behavior of $Na_3Ni_2SbO_6$, to our knowledge. The magnetic susceptibility evolution of $Na_3Ni_2SbO_6$ is also shown in Figure 6. At low temperatures the data indicate a long-range antiferromagnetic ordering with a $T_N \approx 18$ K. At high temperatures, the magnetic susceptibility data follows the Curie-Weiss law and the inverse susceptibility follows a linear trend. The effective magnetic moment for $Na_3Ni_2SbO_6$ is $\mu_{eff}$ = 4.45 $\mu_B$, which is in agreement with the theoretical value assuming $Ni^{2+}$ spin-only contributions ($\mu_{theor}$ = 4.00 $\mu_B$). The Weiss constant is positive (15 K), indicating ferromagnetic short-range interactions. This data is in agreement with the related $Li_3Ni_2BiO_6$ and $Li_3Ni_2SbO_6$ compositions.[24,25] These $Ni^{2+}$ containing compounds both undergo antiferromagnetic ordering transitions at low temperatures with $T_N$ = 5.5 K[25] and 15 K[24], respectively. These compounds also show positive Weiss constants when fit with the Curie-Weiss law from 150 – 300 K which also indicates ferromagnetic interactions at high temperatures. The observed transition for the $Na_3Ni_2SbO_6$ composition is very close to that reported for $Li_3Ni_2SbO_6$ with a $T_N$ = 15 K[24]; however both are higher than that for the $Li_3Ni_2BiO_6$ composition with a $T_N$ = 5.5 K.[25] Since $Bi^{5+}$ (0.76 Å) is larger than $Sb^{5+}$ (0.60 Å), the ionic size affects the $T_N$ for these compounds. The larger $Bi^{5+}$ causes this lower transition temperature because it further separates the $Ni^{2+}$ ions and creates a longer distance for the

$Ni^{2+}$–O–$Ni^{2+}$ superexchange pathway. Based on the Goodenough-Kanamori rules, the 90° angle of the $Ni^{2+}$–O–$Ni^{2+}$ pathway for the $A_3Ni_2SbO_6$ ($A^+$ = Li, Na) indicates ferromagnetic interactions. This superexchange pathway allows for covalent coupling of the $Ni^{2+}$ ions with the two different $p_\sigma$ orbitals of the $O^{2-}$ causing the parallel spins on the $Ni^{2+}$ ions.[41] Since antiferromagnetic interactions are indicated at low temperature, Zvereva *et al.* discusses how the low temperature antiferromagnetic interactions would be arising from antiferromagnetic ordering between the layers.[24] As $Bi^{5+}$ is larger than $Sb^{5+}$, this would decrease the covalencey within the slabs and decrease the $T_N$, which is the result for these compounds.

The magnetic susceptibility evolution for the $Na_3Ni_{2-x}Cu_xSbO_6$ solid solution ($x$ = 0, 0.5, 1, 1.5, 2) can be seen in Figure 6. Upon substitution of $Ni^{2+}$ with $Cu^{2+}$, there are compositionally dependent magnetic contributions from both ions. It is noticed that the short-range antiferromagnetic interactions at low temperature are still present until $x$ = 2, where we only have the $Na_3Cu_2SbO_6$ parent compound with a spin gap behavior. The $\mu_{eff}$ linearly decreases from 4.45 $\mu_B$ for the $Ni^{2+}$ parent phase to 2.33 $\mu_B$ of the $Cu^{2+}$ parent phase. These results agree with the $\mu_{theor}$ for each composition in this $Na_3Ni_{2-x}Cu_xSbO_6$ solid solution for every $x$ = 0 – 2 in increments of 0.5.

The magnetic behavior of the $Na_3Cu_{2-x}M_xSbO_6$ phases (M = Mg or Zn) is shown in Figure 7. The spin gap behavior of the $Na_3Cu_2SbO_6$ parent compound is completely suppressed upon 25% substitution of the non-magnetic ions. This is also noticed in the $Na_3Ni_{2-x}Cu_xSbO_6$ solid solution. The $Cu^{2+}$ dilution lowers the influence of Cu – Cu dimer formations in the $Cu_2SbO_6$ layer. The substitution of $Cu^{2+}$ with other elements disturbs the formation of Cu – Cu dimers and completely disrupts any possibility of the spin gap behavior. The $\mu_{eff}$ for the $Na_3Cu_{2-x}M_xSbO_6$ (M = Mg, Zn) solid solutions for every $x$ = 0 up to $x$ = 1.5, in increments of 0.5, decreases linearly in accordance with $\mu_{theor}$.

The magnetic behavior of $Na_3Ni_{2-x}M_xSbO_6$ (M = Mg, Zn) phases is shown in Figure 8. The substitution of the $Ni^{2+}$ with non-magnetic $M^{2+}$ cations involves a linear dilution of the magnetic moment. The resulting

$\mu_{eff}$ for every $x$ = 0.5 for each non-magnetic ion is in agreement with the theoretical moment for each composition. The long-range antiferromagnetic interaction at low temperature is suppressed with 25% substitution of the non-magnetic ions and is completely gone with higher substitution. This is in agreement with the $Li_3NiM'BiO_6$ (M' = Mg, Zn) magnetic susceptibility results and helps conclude that the antiferromagnetic ground state is from the $Ni^{2+} – O – Ni^{2+}$ interactions.[25]

*3.3 Optical Data:*

Optical studies were performed in order to estimate the band gaps as the color change through the solid solutions indicates a change in this property. The $Cu^{2+}$ and $Ni^{2+}$ end members are green whereas the $Mg^{2+}$ and $Zn^{2+}$ are white. The diffuse reflectance raw data is transformed to absorbance using the Kubelka-Munk relation.[34] The band gap is estimated for each composition by extrapolating the x-intercept at the absorption onset in absorption vs. eV plot. Figure 9 includes the absorbance vs. eV spectra and Table 2 lists the estimated band gaps for each solid solution. It is noticed that the band gap can be tuned depending on the composition even between the white colors of the magnesium and zinc end members. All of the materials are insulating which is in agreement with the large band gaps extrapolated for these solid solutions.

**4. Conclusions:**

This is the first report of the solid solutions for this $Na_3M_2SbO_6$ (M = Cu, Mg, Ni, Zn) family of compounds. The lattice parameter progression within the solid solutions follow an expected linear trend depending on the ionic size of the $M^{2+}$ and $M'^{2+}$ cations (M = Ni; M' = Mg, Zn). For the compositions containing the Jahn-Teller active $Cu^{2+}$ ion the refined β angle decreases as expected upon the substitution of $Mg^{2+}$, $Ni^{2+}$ and $Zn^{2+}$. The low temperature AFM transition for $Na_3Ni_2SbO_6$ disappears upon doping of the non-magnetic $M^{2+}$ cations. The solid solution between $Ni^{2+}$ and $Cu^{2+}$ retain the low temperature antiferromagnetic interactions until the copper end member is reached. The spin gap behavior of $Na_3Cu_2SbO_6$ vanishes with minimal substitution of the other $M^{2+}$, as this behavior is

attributed to ordered Cu – Cu dimers with the honeycomb structure. The estimated band gaps are large which agrees with the fact that these materials are all insulating at room temperature. It is important to explore all aspects of this family of compounds in light of the recent discoveries within this family. They show that these layered materials can be extended to include a vast variety of stoichiometries and many different cations can achieve the honeycomb layering scheme seen in the compounds studied here.

**Acknowledgement**

This work has been supported by NSF grant DMR 0804167. The authors want to thank Geneva Laurita (Oregon State University, Chemistry Department) for technical assistance during the optical measurements.

**Table 1**. Experimental and literature lattice parameters for $Na_3M_2SbO_6$ (M = Cu, Mg, Ni, Zn). *Only LeBail fits were performed in this work. Full refinement for these layered systems is difficult due to stacking defects and low crystallinity. **The lattice parameters reported for the magnesium and zinc compounds were transformed to the monoclinic phase based on the hexagonal parameters reported by Politaev *et al.*

| **Space Group: *C2/m*** | **a (Å)** | **b (Å)** | **c (Å)** | **β (°)** | **Volume (Å$^3$)** | **Reference** |
|---|---|---|---|---|---|---|
| $Na_3Zn_2SbO_6$ | 5.3636(1) | 9.2722(1) | 5.6645(1) | 108.47(1) | 267.20(1) | This work.* |
| | 5.3522 | 9.275 | 5.6718 | 108.34 | | [21]** |
| $Na_3Mg_2SbO_6$ | 5.3285(1) | 9.1908(1) | 5.6711(1) | 108.30(1) | 263.69(1) | This work.* |
| | 5.317 | 9.21 | 5.680 | 108.18 | | [21]** |
| $Na_3Ni_2SbO_6$ | 5.3055(1) | 9.1713(1) | 5.6273(1) | 108.35(1) | 259.89(1) | This work.* |
| | 5.3048(4) | 9.1876(6) | 5.6298(5) | 108.300(8) | | [21]** |
| $Na_3Cu_2SbO_6$ | 5.6691(1) | 8.8448(1) | 5.8252(1) | 113.37(1) | 268.12(1) | This work.* |
| | 5.6759(1) | 8.8659(1) | 5.8379(1) | 113.289(1) | | [16] |

**Table 2.** Estimated band gaps $E_g$ (eV) extrapolated from transformed diffuse reflectance measurements. The band gaps are compositionally dependent.

| | **Extrapolated Band Gaps (eV)** | | | | | |
|---|---|---|---|---|---|---|
| ***x*** | **$Na_3Cu_{2-x}Zn_xSbO_6$** | **$NaCu_{2-x}Mg_xSbO_6$** | **$Na_3Ni_{2-x}Cu_xSbO_6$** | **$Na_3Ni_{2-x}Zn_xSbO_6$** | **$Na_3Ni_{2-x}Mg_xSbO_6$** | **$Na_3Mg_{2-x}Zn_xSbO_6$** |
| 0 | 2.62 | 2.62 | 4.29 | 4.29 | 4.29 | 5.38 |
| 0.5 | 2.89 | 3.11 | 2.86 | 4.20 | 4.41 | - |
| 1 | 2.86 | 3.13 | 2.98 | 4.28 | 4.49 | 4.97 |
| 1.5 | 3.37 | 3.65 | 2.98 | 4.25 | 4.66 | - |
| 2 | 4.49 | 5.38 | 2.62 | 4.49 | 5.38 | 4.49 |

**References:**


[1] K. Mizushima, P.C. Jones, P.J. Wiseman, J.B. Goodenough, Mater. Res. Bull. 15 (1980) 783.

[2] J.-J. Braconnier, C. Delmas, C. Fouassier, P. Hagenmuller, Mater. Res. Bull. 15 (1980) 1797.

[3] C. Delmas, J.-J. Braconnier, C. Fouassier, P. Hagenmuller, Solid State Ionics 3–4 (1981) 165.

[4] R. Berthelot, D. Carlier, C. Delmas, Nat. Mater. 10 (2011) 74.

[5] Y. Takeda, K. Nakahara, M. Nishijima, N. Imanishi, O. Yamamoto, M. Takano, R. Kanno, Mater. Res. Bull. 29 (1994) 659.

[6] J.M. Tarascon, M. Armand, Nature 414 (2001) 359.

[7] M. Armand, J.-M. Tarascon, Nature 451 (2008) 652.

[8] I. Terasaki, Y. Sasago, K. Uchinokura, Phys. Rev. B: Condens. Matter Mater. Phys. 56 (1997) R12685.

[9] K. Takada, H. Sakurai, E. Takayama-Muromachi, F. Izumi, R.A. Dilanian, T. Sasaki, Nature 422 (2003) 53.

[10] C. Delmas, C. Fouassier, P. Hagenmuller, Phys. B 99 (1980) 81.

[11] C. Greaves, S.M.A. Katib, Mater. Res. Bull. 25 (1990) 1175.

[12] J.M.S. Skakle, M.A. Castellanos R., S.T. Tovar, A.R. West, J. Solid State Chem. 131 (1997) 115.

[13] G.C. Mather, R.I. Smith, J.M.S. Skakle, J.G. Fletcher, M.A. Castellanos R, M.P. Gutierrez, A.R. West, J. Mater. Chem. 5 (1995) 1177.

[14] G.C. Mather, C. Dussarrat, J. Etourneau, A.R. West, J. Mater. Chem. 10 (2000) 2219.

[15] R. Nagarajan, S. Uma, M.K. Jayaraj, J. Tate, A.W. Sleight, Solid State Sci. 4 (2002) 787.

[16] O.A. Smirnova, V.B. Nalbandyan, A.A. Petrenko, M. Avdeev, J. Solid State Chem. 178 (2005) 1165.

[17] O.A. Smirnova, M. Avdeev, V.B. Nalbandyan, V.V. Kharton, F.M.B. Marques, Mater. Res. Bull. 41 (2006) 1056.

[18] Y. Miura, R. Hirai, T. Fujita, Y. Kobayashi, M. Sato, J. Magn. Magn. Mater. 310 (2007) e389.

[19] L. Viciu, Q. Huang, E. Morosan, H.W. Zandbergen, N.I. Greenbaum, T. McQueen, R.J. Cava, J. Solid State Chem. 180 (2007) 1060.

[20] S. Derakhshan, J.E. Greedan, T. Katsumata, L.M.D. Cranswick, Chem. Mater. 20 (2008) 5714.

[21] V.V. Politaev, V.B. Nalbandyan, A.A. Petrenko, I.L. Shukaev, V.A. Volotchaev, B.S. Medvedev, J. Solid State Chem. 183 (2010) 684.

[22] E. Climent-Pascual, P. Norby, N.H. Andersen, P.W. Stephens, H.W. Zandbergen, J. Larsen, R.J. Cava, Inorg. Chem. 51 (2011) 557.

[23] M.A. Evstigneeva, V.B. Nalbandyan, A.A. Petrenko, B.S. Medvedev, A.A. Kataev, Chem. Mater. 23 (2011) 1174.

[24] E.A. Zvereva, M.A. Evstigneeva, V.B. Nalbandyan, O.A. Savelieva, S.A. Ibragimov, O.S. Volkova, L.I. Medvedeva, A.N. Vasiliev, R. Klingeler, B. Buechner, Dalton Trans. 41 (2012) 572.

[25] R. Berthelot, W. Schmidt, S. Muir, J. Eilertsen, L. Etienne, A.W. Sleight, M.A. Subramanian, Inorg. Chem. 51 (2012) 5377.

[26] R. Berthelot, W. Schmidt, A.W. Sleight, M.A. Subramanian, J. Solid State Chem. 196 (2012) 225.

[27] V. Kumar, N. Bhardwaj, N. Tomar, V. Thakral, S. Uma, Inorg. Chem. 51 (2012) 10471.

[28] V.B. Nalbandyan, M. Avdeev, M.A. Evstigneeva, J. Solid State Chem. 199 (2013) 62.

[29] V.B. Nalbandyan, A.A. Petrenko, M.A. Evstigneeva, Solid State Ionics 233 (2013) 7.

[30] E.A. Zvereva, O.A. Savelieva, Y.D. Titov, M.A. Evstigneeva, V.B. Nalbandyan, C.N. Kao, J.-Y. Lin, I.A. Presniakov, A.V. Sobolev, S.A. Ibragimov, M. Abdel-Hafiez, Y. Krupskaya, C. Jähne, G. Tan, R. Klingeler, B. Büchner, A.N. Vasiliev, Dalton Trans. 42 (2013) 1550.

[31] J. Rodríguez-Carvajal, Physica B: Condensed Matter 192 (1993) 55.

[32] J. Rodriguez-Carvajal, T. Roisnel, Internation Union for Crystallography, Newsletter 20 (1998).

[33] T. Roisnel, J. Rodriguez-Carvajal, Prodeedings of the Seventh European Powder Diffraction Conference (EPDIC 7) (2000) 118.

[34] P. Kubelka, F. Munk,, Z. Tech. Phys. 12 (1931) 593.

[35] R.D. Shannon, Acta Crystallogr., Sect. A: Found. Crystallogr. 32 (1976) 751.

[36] J. Bréger, M. Jiang, N. Dupré, Y.S. Meng, Y. Shao-Horn, G. Ceder, C.P. Grey, J. Solid State Chem. 178 (2005) 2575.

[37] A. Boulineau, L. Croguennec, C. Delmas, F. Weill, Solid State Ionics 180 (2010) 1652.

[38] Y. Miura, R. Hirai, Y. Kobayashi, M. Sato, J. Phys. Soc. Jpn. 75 (2006) 084707.

[39] H.-J. Koo, M.-H. Whangbo, Inorg. Chem. 47 (2007) 128.

[40] J. Xu, A. Assoud, N. Soheilnia, S. Derakhshan, H.L. Cuthbert, J.E. Greedan, M.H. Whangbo, H. Kleinke, Inorg. Chem. 44 (2005) 5042.

[41] J.B. Goodenough, Magnetism and the Chemical Bond, John Wiley & Sons: Interscience Publishers, New York-London, 1963.

**Figure and Table Captions:**

**Figure 1**. Representation of the O3-$Na_3M_2SbO_6$ structure. Left: Perspective along the *b* direction, indicating the stacking of the $M_{2/3}Sb_{1/3}O_2$ slabs with the $Na^+$ cations filling the octahedral interslab voids and the β angle between the *a* and *c* directions. Right: Perspective along the *c* direction, indicating the honeycomb ordering within the $M_{2/3}Sb_{1/3}O_2$ slabs with six $MO_6$ octahedra surrounding one $SbO_6$ octahedra. All the octahedral in this structure are edge sharing.

**Figure 2.** PXRD patterns of all O3-$Na_3M_2SbO_6$ where M = Cu, Mg, Ni, Zn. All patterns were indexed to the monoclinic space group *C2/m*. A broad asymmetry in the 17° to 30° 2θ region indicates the presence of some concentration of stacking faults in the Mg, Ni and Zn compounds. The reduced intensities for the Ni and Zn patterns in this region is related to low crystallinity and stacking faults that affect these *hkl* reflections. The dramatic shifting of the *hkl* reflections in the Cu compounds is caused by the Jahn-Teller distortion of the $CuO_6$ octahedra.

**Figure 3.** PXRD patterns for $Na_3Ni_{2-x}Mg_xSbO_6$ solid solution for $x$ = 0, 0.5, 1, 1.5, 2. The slight shifting of the *hkl* positions is due to the ionic radius of the respective $M^{2+}$ present here.

**Figure 4a-b.** a) PXRD patterns for solid solution $Na_3Cu_{2-x}Zn_xSbO_6$, the highlighted section indicates the 2θ region that is highly affected by the transition from regular $ZnO_6$ octahedra to Jahn-Teller distorted $CuO_6$ octahedra. b) Evolution of the highly affected *hkl* positions resulting from the regular $ZnO_6$ octahedra vs. the J-T distorted $CuO_6$ octahedra within the monoclinic structure of the end member compositions.

**Figure 5a-b**. Lattice parameter evolution for the solid solution $Na_3Cu_{2-x}Zn_xSbO_6$ for $x$ = 0, 0.5, 1. 1.5, 2. a) Evolution of the β angle as the Jahn-Teller active $Cu^{2+}$ is diluted. b) Linear trends of the *a*, *b*, and *c* lattice paramteters, the direction of the lattice parameter shifting is a result of the distortion from J-T $Cu^{2+}$ and

is opposite of what would be expected from the ionic radii. The error bars associated with these data points are smaller than the data markers.

**Figure 6.** Magnetic susceptibility, χ vs. T, for $Na_3Ni_{2-x}Cu_xSbO_6$ with an inset showing the 1/χ vs. T plot for this solid solution. The high temperature data follows the Curie-Weiss law and is fit from 150 – 300 K to determine the $\mu_{eff}$ for each composition. The $T_N$ present due to the $Na_3Ni_2SbO_6$ phase (pink line) slightly shifts to lower temperatures and disappears only at the $Na_3Cu_2SbO_6$ parent compound. The copper parent phase (blue line) indicates spin gap behavior which has been thoroughly discussed and reported previously.

**Figure 7a-b.** Magnetic susceptibility, χ vs. T, for $Na_3Cu_{2-x}M_xSbO_6$ (M = Mg, Zn) with an inset showing the 1/χ vs. T plot for these solid solutions. The high temperature data follows the Curie-Weiss law and is fit using $\chi = C/(T - \theta)$ from 150 – 300 K to determine the $\mu_{eff}$ for each composition. The spin gap behavior present due to the $Na_3Cu_2SbO_6$ phase (blue line) disappears upon substitution.

**Figure 8a-b.** Magnetic susceptibility, χ vs. T, for $Na_3Ni_{2-x}M_xSbO_6$ (M = Mg, Zn) with an inset showing the 1/χ vs. T plot for these solid solutions. The high temperature data follows the Curie-Weiss law and is fit from 150 – 300 K by $\chi = C/(T - \theta)$, to determine the $\mu_{eff}$ for each composition. The $T_N$ present due to the $Na_3Ni_2SbO_6$ phase (blue line) slightly shifts to lower temperatures and disappears after 25% dilution with non-magnetic ions.

**Figure 9.** Transformed diffuse reflectance spectra in absorbance vs. eV for each $Na_3M_{2-x}M'_xSbO_6$ (M, M' = Cu, Mg, Ni, Zn) solid solution. The band gaps were extrapolated from the initial absorption onset to get the x-intercept.

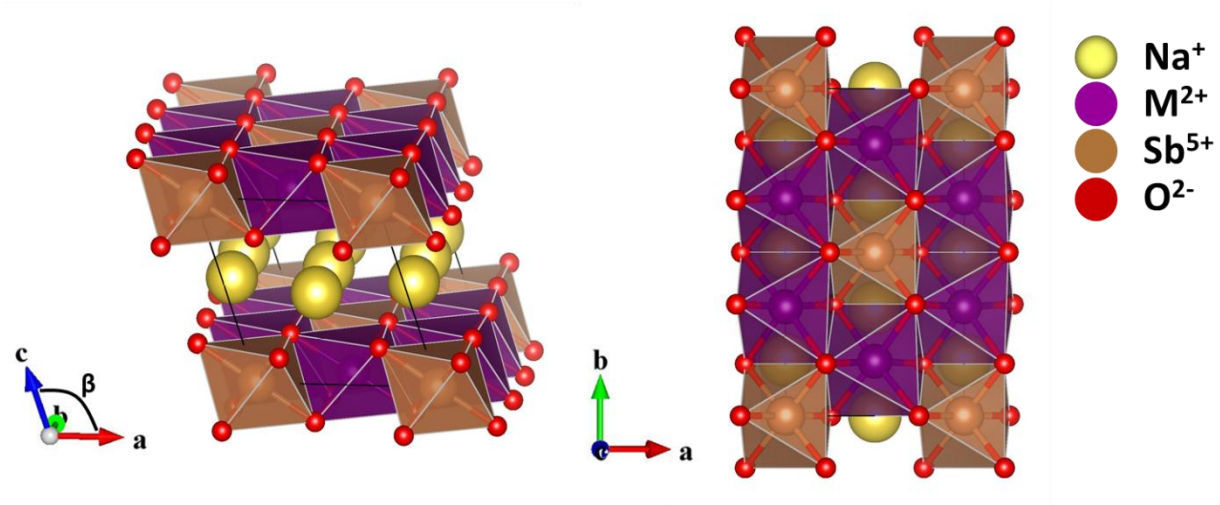


**Figure 1.**

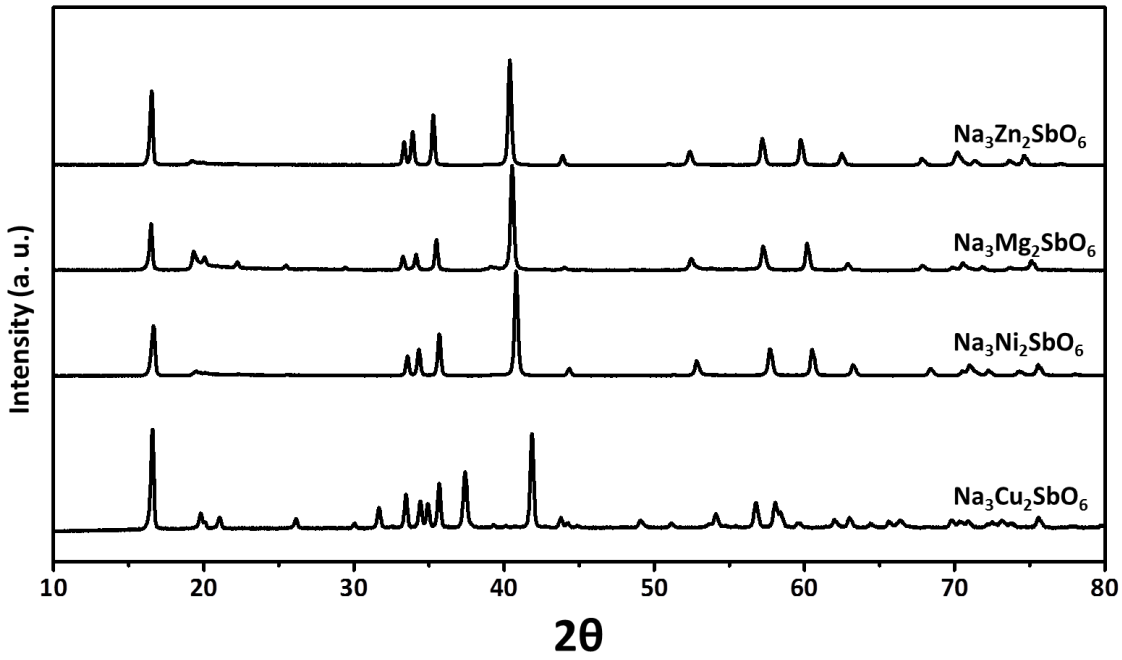
Intensity (a. u.)
Na3Zn2SbO6
Na3Mg2SbO6
Na3Ni2SbO6
Na3Cu2SbO6
10
20
30
40
50
60
70
80
2θ

**Figure 2.**

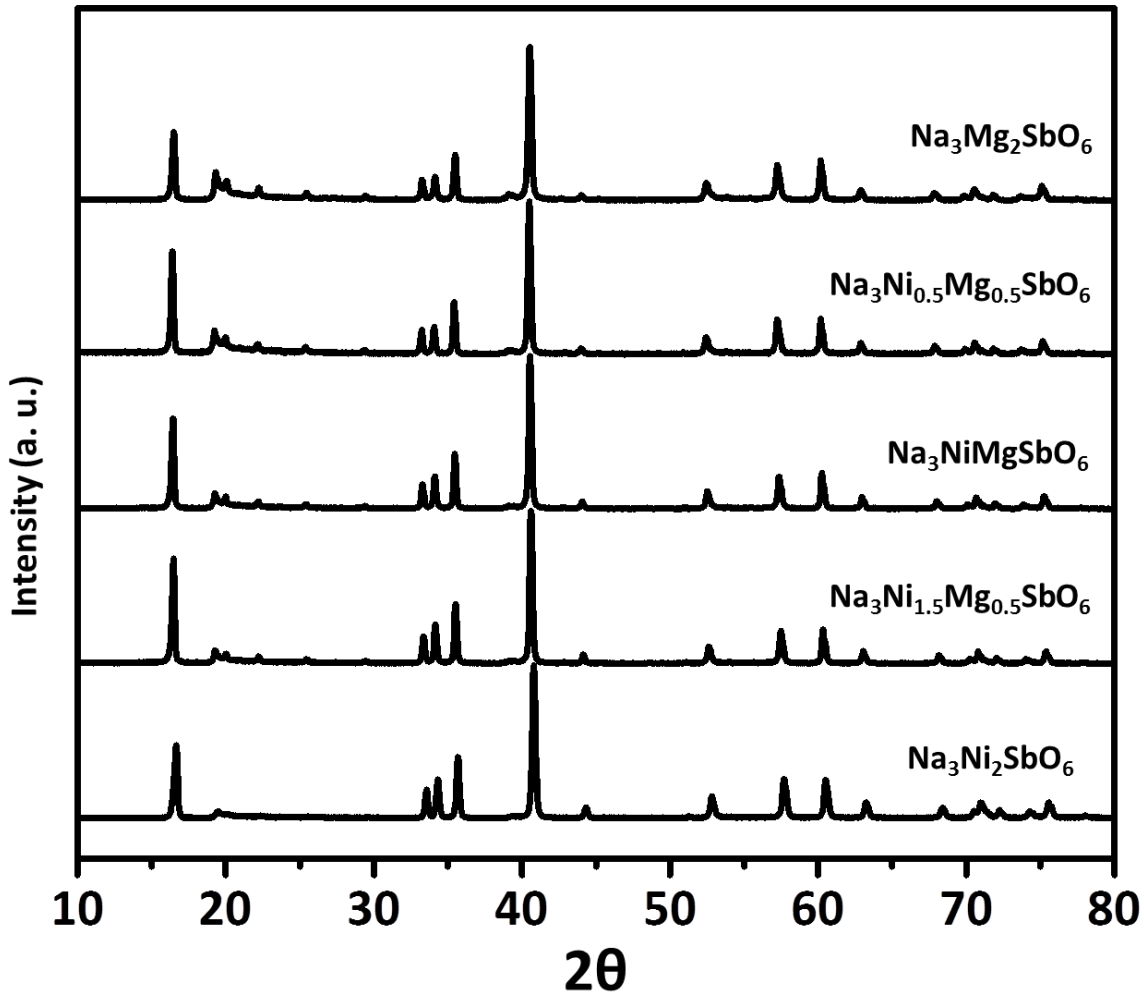
Na3Mg2SbO6
Na3Ni0.5Mg0.5SbO6
Na3NiMgSbO6
Na3Ni1.5Mg0.5SbO6
Na3Ni2SbO6
Intensity (a. u.)
10
20
30
40
50
60
70
80
2θ

**Figure 3.**

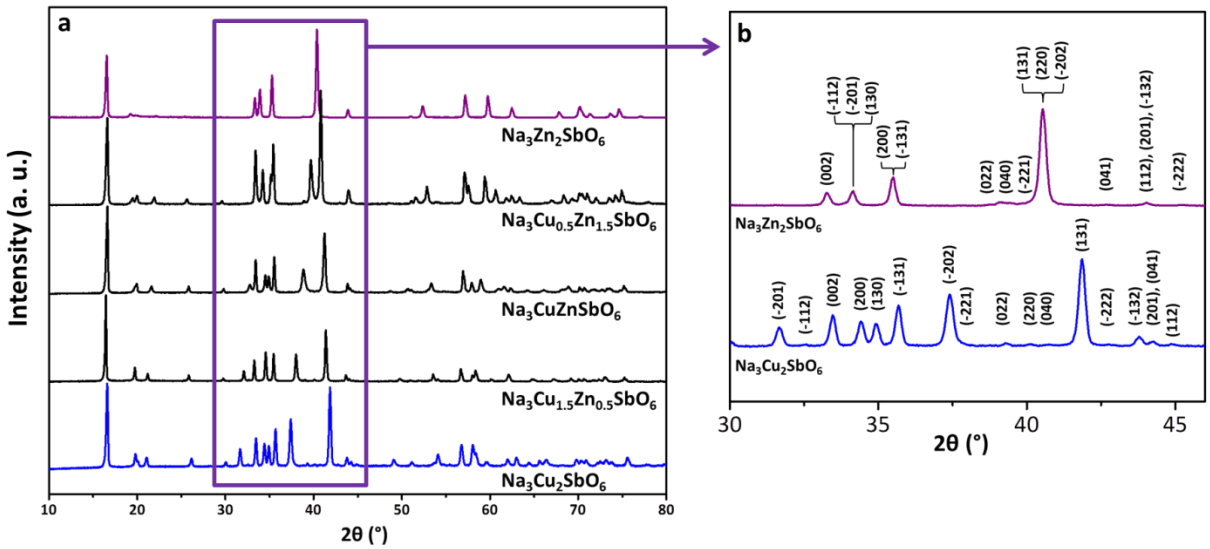
a
b
Intensity (a. u.)
2θ (°)
Na3Zn2SbO6
Na3Cu0.5Zn1.5SbO6
Na3CuZnSbO6
Na3Cu1.5Zn0.5SbO6
Na3Cu2SbO6
(002)
(-112)
(-201)
(130)
(200)
(-131)
(022)
(040)
(-221)
(131)
(220)
(-202)
(041)
(112), (201), (-132)
(-222)
(-201)
(-112)
(002)
(200)
(130)
(-131)
(-202)
(-221)
(022)
(220)
(040)
(131)
(-222)
(-132)
(201), (041)
(112)

**Figure 4.**

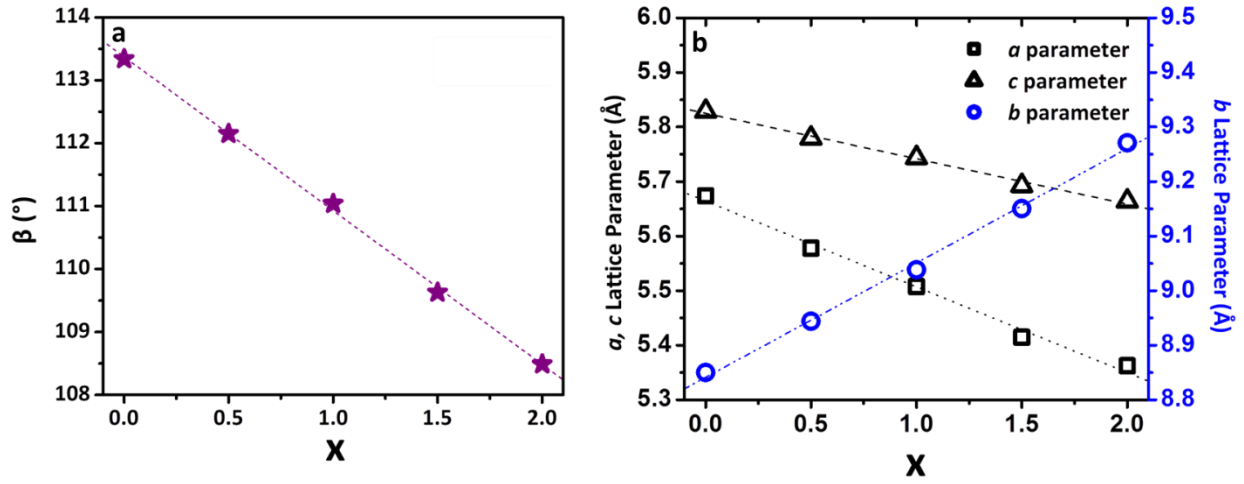
a
β (°)
X
b
a parameter
c parameter
b parameter
a, c Lattice Parameter (Å)
b Lattice Parameter (Å)
X

**Figure 5a-b**

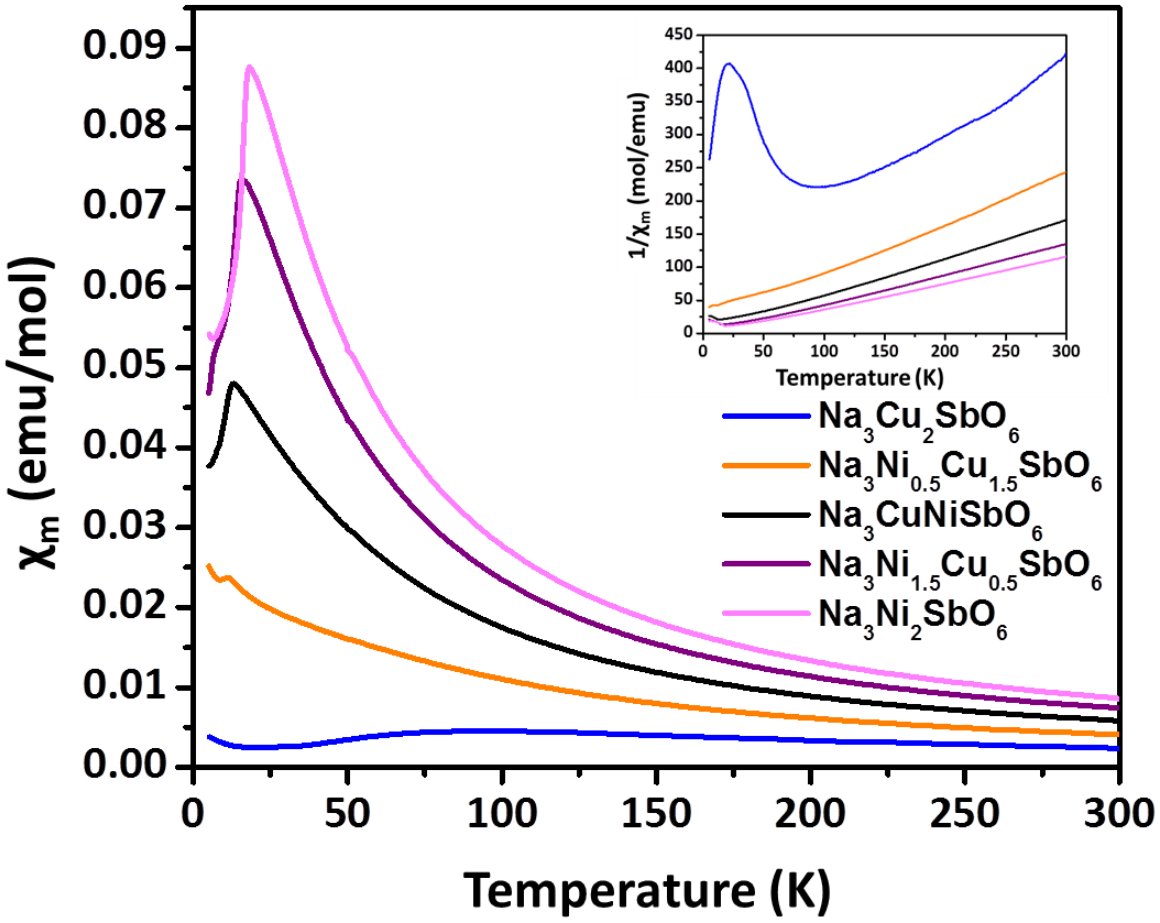
χm (emu/mol)
Temperature (K)
1/χm (mol/emu)
Temperature (K)
Na3Cu2SbO6
Na3Ni0.5Cu1.5SbO6
Na3CuNiSbO6
Na3Ni1.5Cu0.5SbO6
Na3Ni2SbO6

**Figure 6.**

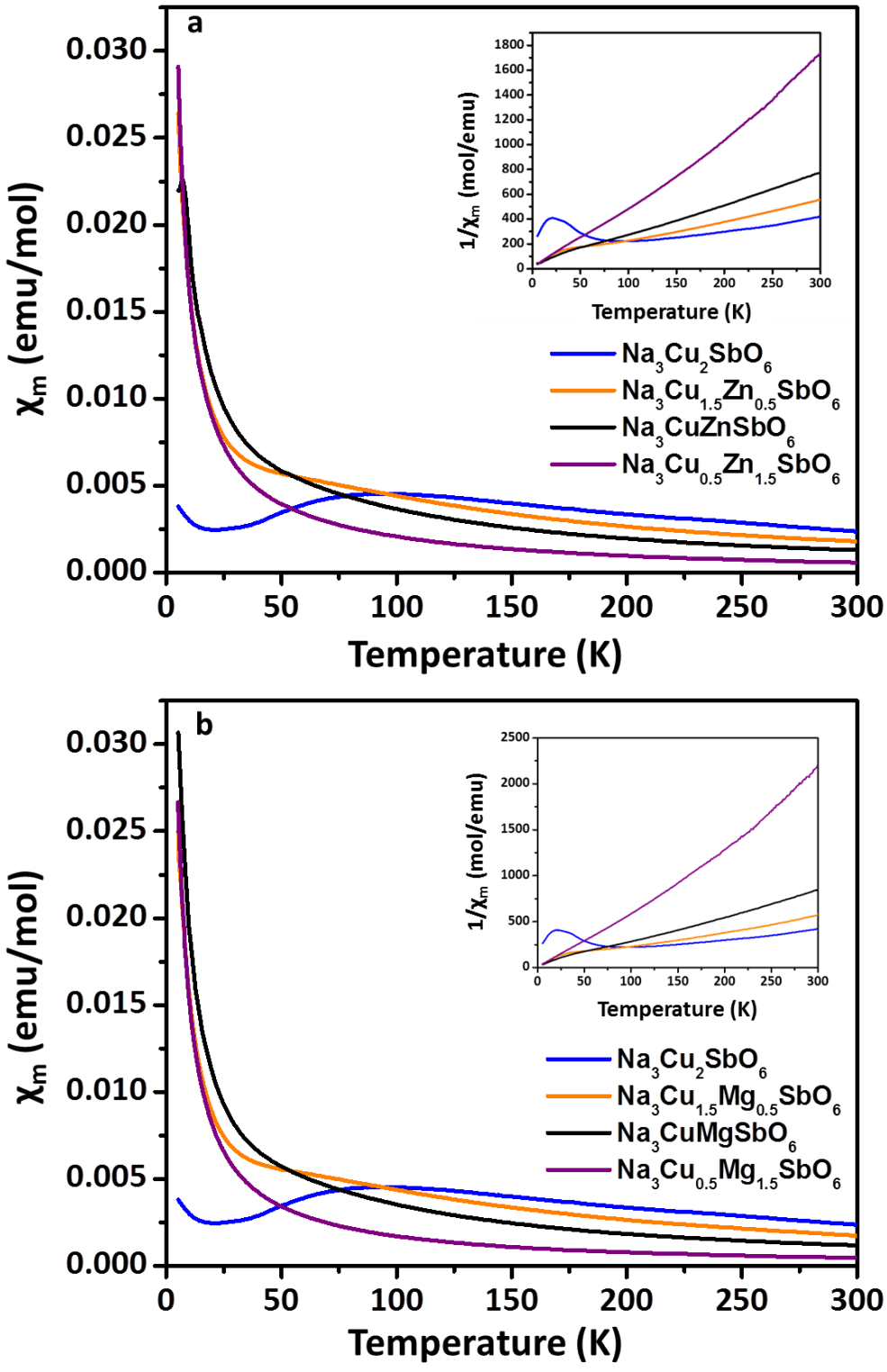
a
χm (emu/mol)
Temperature (K)
1/χm (mol/emu)
Na3Cu2SbO6
Na3Cu1.5Zn0.5SbO6
Na3CuZnSbO6
Na3Cu0.5Zn1.5SbO6
b
χm (emu/mol)
Temperature (K)
1/χm (mol/emu)
Na3Cu2SbO6
Na3Cu1.5Mg0.5SbO6
Na3CuMgSbO6
Na3Cu0.5Mg1.5SbO6

**Figure 7a-b.**

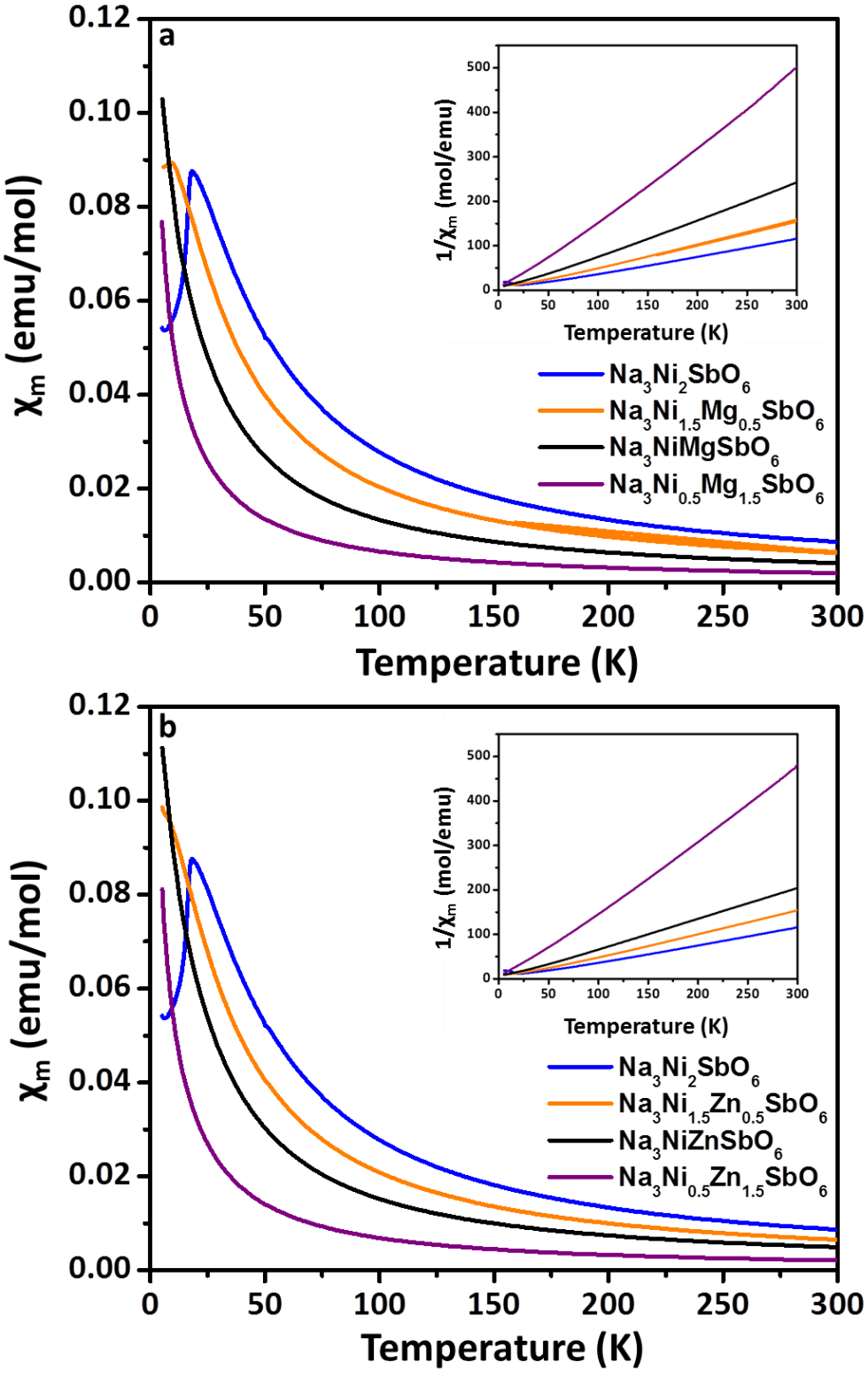
a
$\chi_m$ (emu/mol)
Temperature (K)
1/$\chi_m$ (mol/emu)
Temperature (K)
$Na_3Ni_2SbO_6$
$Na_3Ni_{1.5}Mg_{0.5}SbO_6$
$Na_3NiMgSbO_6$
$Na_3Ni_{0.5}Mg_{1.5}SbO_6$
b
$\chi_m$ (emu/mol)
Temperature (K)
1/$\chi_m$ (mol/emu)
Temperature (K)
$Na_3Ni_2SbO_6$
$Na_3Ni_{1.5}Zn_{0.5}SbO_6$
$Na_3NiZnSbO_6$
$Na_3Ni_{0.5}Zn_{1.5}SbO_6$

**Figure 8a-b**

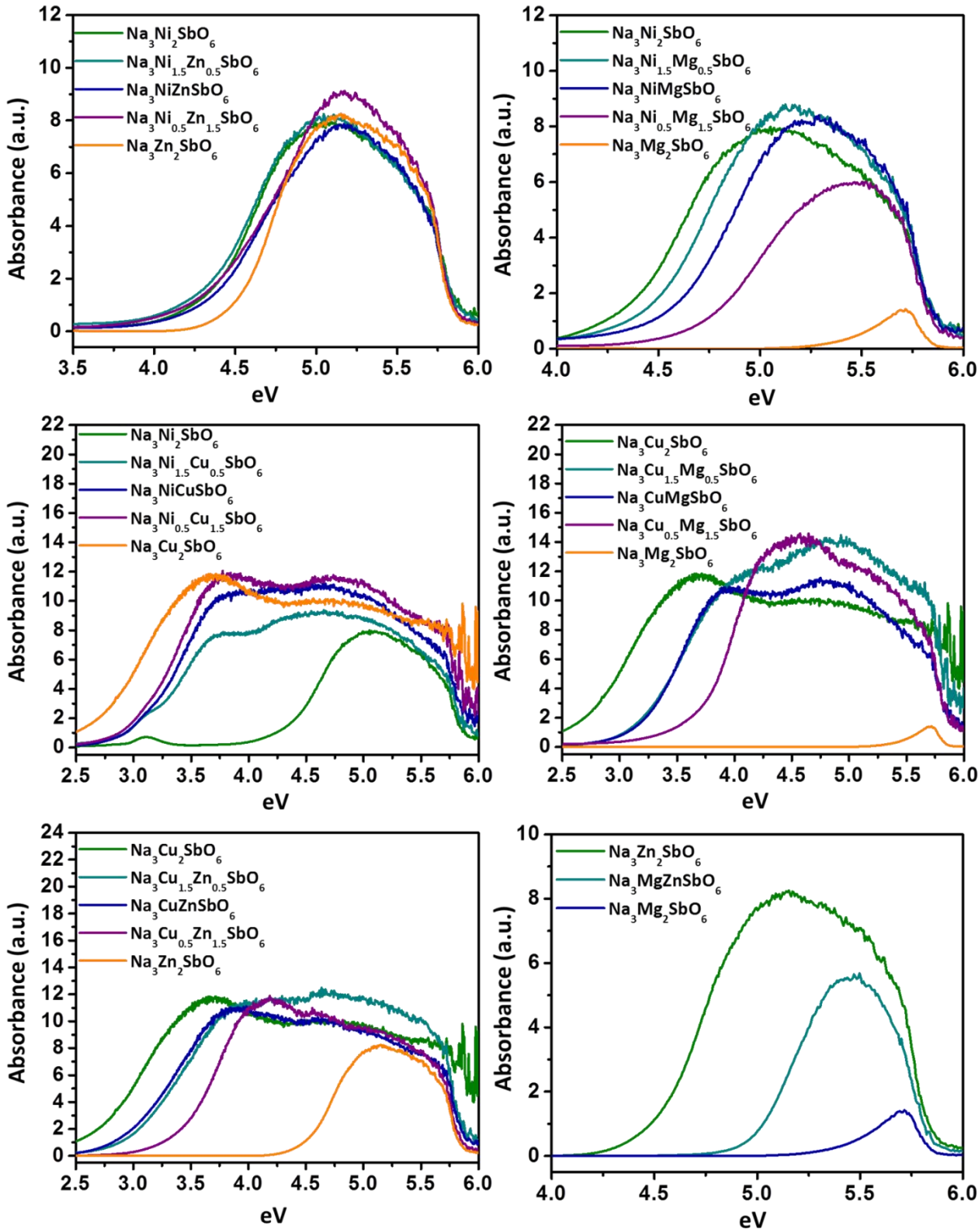
Na3Ni2SbO6
Na3Ni1.5Zn0.5SbO6
Na3NiZnSbO6
Na3Ni0.5Zn1.5SbO6
Na3Zn2SbO6
Na3Ni2SbO6
Na3Ni1.5Mg0.5SbO6
Na3NiMgSbO6
Na3Ni0.5Mg1.5SbO6
Na3Mg2SbO6
Na3Ni2SbO6
Na3Ni1.5Cu0.5SbO6
Na3NiCuSbO6
Na3Ni0.5Cu1.5SbO6
Na3Cu2SbO6
Na3Cu2SbO6
Na3Cu1.5Mg0.5SbO6
Na3CuMgSbO6
Na3Cu0.5Mg1.5SbO6
Na3Mg2SbO6
Na3Cu2SbO6
Na3Cu1.5Zn0.5SbO6
Na3CuZnSbO6
Na3Cu0.5Zn1.5SbO6
Na3Zn2SbO6
Na3Zn2SbO6
Na3MgZnSbO6
Na3Mg2SbO6
Absorbance (a.u.)
eV

**Figure 9.**